Deep–Sea Research II 199 (2022) 105080

Contents lists available at ScienceDirect

Deep-Sea Research Part II

journal homepage: www.elsevier.com/locate/dsr2

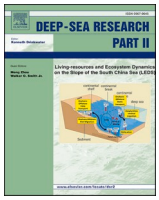

Drivers of productivity on the Agulhas Bank and the importance for marine ecosystems

Zoe Jacobs [a,*], Mike Roberts [a,b], Fatma Jebri [a], Meric Srokosz [a], Stephen Kelly [a], Warwick Sauer [c], Jorn Bruggeman [d,e], Ekaterina Popova [a]

[a] National Oceanography Centre, Southampton, SO14 3ZH, United Kingdom
[b] Nelson Mandela University, Gqeberha, 6001, South Africa
[c] Department of Ichthyology and Fisheries Science, Rhodes University, Makhanda, South Africa
[d] Bolding & Bruggeman ApS, Asperup, Denmark
[e] Plymouth Marine Laboratory, Plymouth, UK

ARTICLE INFO

Keywords:
Agulhas Bank
South Africa
Model
Cold ridge
Upwelling
Advection
Productivity
Chokka squid

ABSTRACT

The Agulhas Bank, an area of broad continental shelf extending 250 km offshore of South Africa, sustains rich and productive fisheries. However, its primary production is driven by a complex mosaic of biophysical mechanisms, highly variable in time and space. The key drivers include a system of multiple costal upwellings, complex shelf currents and an interaction with the powerful Agulhas current. The patterns of spatial and temporal variability of primary production on the Agulhas Bank are critical for the spawning and survival of early life stages of many commercially important species exploited along the coastline of South Africa. In particular, the 'chokka' squid fishery is an important source of revenue for the Eastern Cape coastal region in South Africa, with low catch years causing socioeconomic hardship. After spawning on the Eastern Agulhas Bank, the squid paralarvae are thought to be transported west to the Central Agulhas Bank (CAB). This region is associated with a cool, productive, but rather intermittent, oceanic feature known as the 'cold ridge' (CR). If and when it occurs, this feature could provide a sufficient amount of concentrated (relative to the background values) food for the paralarvae to survive during its passive or near-passive stage. To date, a long-term analysis of CR variability and the mechanisms associated with this has not been conducted. Here, we used a high-resolution biogeochemical ocean model (NEMO-MEDUSA) to investigate the drivers of the productivity on the Agulhas Bank, specifically in the vicinity of the CR. Evidence of the CR is found from November to April and variability in its strength and spatial extent is comparable to that observed in remote sensing data. Interannual variability in productivity on the CAB is correlated to wind stress and zonal currents with the most productive events associated with anomalous easterly winds and enhanced westward flow on the Bank. These events coincide with the existence of an intense CR, important for overall productivity on the Bank, which may impact the recruitment of chokka squid and other fish species. From this simulation, we observe a season of low productivity in 2012 which may potentially relate to the infamous low catch in 2013 which caused economic hardship in the area.

1. Introduction

The Agulhas Bank ('the Bank') is an area of broad continental shelf extending 250 km offshore of South Africa, from 18 to 29°E (Fig. 1; Largier and Swart, 1987). It plays a vital role in supporting many of the country's economically important fisheries such as anchovies, sardines and 'chokka' squid (e.g., Augustyn et al., 1994; Hutchings et al., 1998; Roy et al., 2007). In particular, the chokka squid, *Loligo reynaudii*, fishery employs around 3000 people in the Eastern Cape (DAFF, 2009, currently DFFE). The fishery suffered a major decline in 2013 with catches plummeting by 80%, devastating the livelihoods of those dependent on it (Joyner, 2015; Mthembu, 2019). The cause of the low catch remains unclear. However, different stages of the life cycle of chokka squid are influenced by environmental conditions (Roberts, 2005) and these may affect the annual catch, making it imperative to understand what drives productivity on the Agulhas Bank.

Chokka spawn on the Eastern Agulhas Bank (EAB) from 24 to 27°E (Fig. 1) where bottom temperatures and dissolved oxygen

* Corresponding author.
E-mail address: zoe.jacobs@noc.ac.uk (Z. Jacobs).

https://doi.org/10.1016/j.dsr2.2022.105080
Received 11 June 2021; Received in revised form 3 March 2022; Accepted 28 March 2022
Available online 19 April 2022

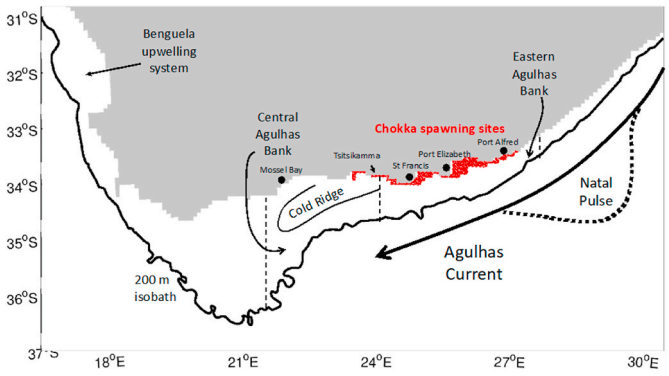

Fig. 1. Map of South Africa highlighting the Agulhas Bank, delineated by the 200 m isobath. A major oceanographic feature known as the 'cold ridge' is shown. Red shaded area demarcates the main chokka squid spawning grounds. The Natal Pulse which forces the current core offshore is schematically shown.

concentrations are optimal for egg development during the austral summer (Roberts, 2005). These conditions exist due to the upwelling of South Indian Ocean central water that occurs via multiple mechanisms (e.g., Swart and Largier, 1987; Russo et al., 2019). The powerful Agulhas Current flows poleward along the edge of the Agulhas Bank, defined by the 200 m isobath, which initiates Ekman transport in the bottom boundary layer, causing cold, nutrient-rich water to flow onto the shelf (Hsuesh and O'Brien, 1971; Gill and Schumann, 1979; Schumann, 1986; Swart and Largier, 1987). This occurs year-round, with a faster Agulhas Current leading to enhanced flow onto the shelf (Roughan and Middleton, 2002; Lutjeharms, 2006; Russo et al., 2019). This upwelled water does not reach the surface but rather forms a bottom layer that is easily upwelled in the near coastal waters driven by the strong austral summer (November–April) easterly winds (Beckley, 1983; Schumann et al., 1982; Roughan and Middleton 2002; Leber et al., 2017). Consequently, low sea surface temperatures (SSTs) are well correlated with these summer easterly winds (Schumann et al., 1995; Malan et al., 2019), with observed temperature decreasing down to 11°C during particularly strong upwelling events (Schumann et al., 1988; Lutjeharms et al., 2000; Goschen et al., 2012). High nutrient concentrations are also found at the surface during these events (e.g., Lutjeharms et al., 1996), initiating enhanced primary production (Barlow et al., 2010).

In addition to seasonal coastal wind-driven upwelling, meanders, eddies and Natal Pulses along the inshore boundary of the Agulhas Current can also lead to episodic upwelling events on the EAB (Chapman and Largier 1989; Lutjeharms et al., 1989; Bryden et al., 2005). Natal Pulses are large, solitary, transient meanders that form in the upper reaches of the Agulhas Current near the Natal Bight and travel southward (Fig. 1; De Ruijter et al., 1999; Lutjeharms et al., 2000; Rouault and Penven, 2011). Their occurrence varies from year to year with an average of 1.6 per year (Rouault and Penven, 2011), but up to five have been recorded in a single year (Yamagami et al., 2019). The arrival of a Natal Pulse near the Agulhas Bank causes the Agulhas Current to move offshore by up to 200 km (Rouault and Penven, 2011), causing divergent upwelling on the shelf that can last for >7 days (Goschen et al., 2015). The different upwelling mechanisms are well observed and understood but their biological impact remains unclear.

While upwelling conditions on the EAB are suitable for chokka spawning, conditions on the rest of the Bank determine the chances of survival for the paralarvae. After hatching, the chokka paralarvae are thought to be advected westward in the prevailing currents (Roberts and Van den Berg, 2005) to the Central Agulhas Bank (CAB) where productivity is higher, mainly due to the existence of the cold ridge (CR; Roberts, 2005). The CR is a quasi-permanent productive filament, first observed by Swart and Largier (1987) in March 1986, that appears to be important for recruitment of various species (e.g., Parada et al., 2003; Miller et al., 2006). It tends to be found on the CAB between Cape St Francis and Mossel Bay in the summer and autumn (November–April), and is observed in cruise surveys and satellite imagery to be roughly aligned with the curvature of the 100 m isobath (Swart and Largier, 1987; Hutchings, 1992; Peterson et al., 1992; Boyd and Shillington, 1994; Roberts and Van den Berg, 2002). In hydrographic sections, the CR is identified by an upward doming of isotherms which often break the surface (e.g., Boyd and Shillington, 1994). However, it can also remain a subsurface feature (Swart and Largier, 1987; Boyd and Shillington, 1994), at times resulting in a subsurface chlorophyll-a maximum (Shannon et al., 1984; Probyn et al., 1994). A few oceanographic surveys conducted on the Agulhas Bank indicate that a high density of copepods is found in the vicinity of the CR, which could suggest abundant food for chokka squid paralarvae (Huggett and Richardson, 2000). Roberts (2005) proposed that a decline in CR strength could increase the risk of starvation for the chokka paralarvae and reduce recruitment the following year, which could reduce biomass and overall catch.

As previously indicated, the CR occurs mainly during the summer upwelling season when strong stratification occurs on the Bank. This is caused by solar-induced warming of the surface water above the cold bottom water (Boyd et al., 1985; Lutjeharms et al., 1996; Russo et al., 2019). In winter, the strong westerly winds lead to enhanced vertical mixing which erodes the sharp thermocline, preventing the formation of the CR (Schumann, 1992). However, even under intense summer upwelling conditions, the CR does not always form, suggesting other dynamics are at play (Roberts, 2005). Previous studies have focussed on mechanisms responsible for the cold bottom water on the shelf, namely shelf-edge upwelling in the bottom layer near Port Alfred on the EAB and further west at the edge of the CAB (Chang, 2008; Jackson et al., 2012). In particular, Chang (2008) performed a numerical modelling experiment that revealed that the existence of the Agulhas Current is vital for shelf-edge upwelling to occur, and thus a primary mechanism for the formation of the CR. Seasonal analysis also indicated that the strongest surface expression occurs in summer, which is likely due to increased shelf-edge upwelling from a faster Agulhas Current and wind-induced upwelling enabling doming of the thermocline (Chang, 2008). The westward widening of the shelf and concomitant shelf flow has also been suggested as a mechanism, resulting in central divergent upwelling around the position of the CR (Boyd and Shillington, 1994). A third mechanism has also been hypothesised as a potential driver in CR formation - the westward flow on the Bank (Roberts, 2005). In addition to transporting chokka paralarvae westwards, currents on the Bank may be important in advecting the nutrient-rich water upwelled on the EAB towards the CAB, further enhancing phytoplankton blooms in the CR (e.g., Swart and Largier, 1987; Boyd and Shillington, 1994; Roberts, 2005; Chang, 2008).

Thus far, studies that identify the CR are generally based on a small collection of observational surveys that only look at the end of winter or early spring. Chang (2008) used a numerical model climatology to understand the seasonality of the CR and the mechanisms associated with its formation, namely shelf-edge upwelling induced from the Agulhas Current. Here, we use a new approach, utilizing a high-resolution biogeochemical ocean model hindcast (>20 years) to address the following questions: i) What is the spatial pattern of productivity on the Agulhas Bank? ii) What is the seasonal and interannual variability of this productivity? iii) Is it possible to model the CR and is it important for the overall productivity on the Bank? And iv) What roles do wind and advection play in driving variations of the CR and, thus, overall productivity on the CAB?

2. Methods

2.1. Model

This study utilizes version 3.6 of the global ocean model Nucleus for European Modelling of the Ocean (NEMO), which uses a series of global

grid configurations (ORCA) at various spatial resolutions (Madec, 2015). The high spatial resolution of the ORCA12 hindcast, 1/12° (Marzocchi et al., 2015; Moat et al., 2016; Jacobs et al., 2020), corresponds to approximately 9.25 km at the equator and 7.5 km at 35°S. The model has 75 vertical levels which become thinner near the surface, i.e., the surface level is < 1 m, there are 22 levels in the upper 100 m and at 5500 m the thickness is ~250 m. The bottom topography, derived from ETOPO2 (a global gridded relief dataset), is represented as partial steps (US Department of Commerce, 2006).

The simulation is initialized using climatological fields from the World Ocean Database (Levitus et al., 1998) and is forced by the Drakkar Surface Forcing dataset version 5.2, which supplies 3-hourly 2 m air temperature, 2 m humidity and 10 m winds and daily surface radiative fluxes and precipitation, at 0.7° horizontal resolution (Brodeau et al., 2010; Dussin et al., 2016). It should be noted that this relatively coarse resolution may have implications for the model's ability to resolve wind-driven upwelling at the coast (see section 3.1). Sea surface salinity is moderately relaxed towards the climatology (Antonov et al., 2006) with a 180-day timescale to avoid excessive drift in global salinity. The hindcast used in this study covers the time period 1958 to 2015 with model output stored as 5-day means.

The biogeochemistry is represented by MEDUSA-2 embedded in NEMO and were run for 26 years from 1990 to 2015 (Yool et al., 2013). This is a size-based, intermediate complexity model that divides the plankton community into two components, "small" and "large", and resolves the elemental cycles of nitrogen, iron and silicon. The "small" component of the ecosystem represents the microbial loop of microzooplankton and picophytoplankton, while the "large" component represents mesozooplankton and microphytoplankton (specifically diatoms). The non-living particulate detritus pool is similarly split between large, fast-sinking particles that are represented only implicitly and small, slow-sinking particles that are simulated explicitly. A full description of MEDUSA-2 is given in Yool et al. (2013) The physical and biogeochemical components of the model have been extensively validated at the global and regional scales, including the Indian Ocean (e.g., Srokosz et al., 2015; Popova et al., 2016; Jacobs et al., 2020). Here, to ensure consistency between the physics and biogeochemistry, and to also avoid the spin-up period of MEDUSA during the early 1990s, monthly means from the period 1993–2015 are analysed.

2.2. Lagrangian experiments

To investigate advection timescales between the EAB and CAB, Lagrangian experiments were run using the particle tracking tool *Ariane*, an offline mass-preserving Lagrangian scheme that uses an analytical method to calculate three-dimensional streamlines of the velocity fields (Blanke and Raynaud, 1997). Five-day means of the 3D velocity fields from the NEMO hindcast were used as input data to disperse virtual particles in the model flow field, interpolating through model grid cells to ensure effective particle translation, with particles' positions stored daily. Monthly experiments were performed from 1995 to 2013 (a total of 226 experiments) with particles initialized at the beginning of each month and allowed to travel in the model 3D velocity field. Particles were considered to be neutrally buoyant with no additional movement representing biological behaviour. To represent the main chokka spawning sites (Lipinski et al., 2016), particles were released at the surface from 23.5 to 27°E along the coast where depths are shallower than 60 m (Fig. 1). Particles were uniformly distributed in latitude and longitude with a total of 1470 released per experiment, with trajectories tracked for 100 days.

2.3. Observational datasets

Surface geostrophic velocities from the multi-satellite gridded and merged AVISO (Archiving, Validation and Interpretation of Satellite Oceanographic Data) altimetry product distributed by the Copernicus Marine Environment Monitoring Service (http://marine.copernicus.eu/services-portfolio/access-to-products/?option=com_csw&view=details&product_id=SEALEVEL_GLO_PHY_L4_REP_OBSERVATIONS_008_047) were used to assess the large-scale performance of modelled currents. The data consist of the delayed-time "Update" DUACS-DT2018 version. Geostrophic zonal and meridional velocities are computed weekly on a 1/4° × 1/4° grid.

Monthly satellite observations of SST were taken from the European Space Agency (ESA) Climate Change Initiative (CCI), which uses a multi-sensor approach (AVHRRs and ATSR) to create a global database from 1991 to 2010 (http://www.esa-sst-cci.org/) with a spatial resolution of 4 km.

Satellite chlorophyll-*a* (chl-*a*) observations were taken from the ESA Ocean Colour CCI (OC–CCI; v.3.1), which is one of the most complete, validated, multi-sensor (MODIS-Aqua, SeaWiFS and MERIS) global datasets of ocean colour available (Racault et al., 2017). Here, monthly means, at 4 km spatial resolution, were used from 1997 to 2017 (http://www.esa-oceancolour-cci.org/). It should be noted that satellite chlorophyll observations have known limitations, especially in shallow optically complex Case II waters where suspended sediments, particulate matter and/or dissolved organic matter do not co-vary in a predictable manner with chlorophyll (IOCCG and Sathyendrannath, 2000). Despite OC-CCI using a multi-chlorophyll algorithm approach (see Jackson et al., 2017 for more details), satellite chl-*a* observations over the study region may be over-estimated in shallow waters along the South African coast. As the majority of the area included in this study comprises Case-I open waters, this bias influences only a small proportion of the data points.

Modelled depth-integrated primary productivity (IntPP) is compared with an average (following Yool et al., 2015 and Popova et al., 2016) from three satellite-derived estimates, the Vertically Generalized Production Model (VGPM) (Behrenfeld and Falkowski, 1997), the Eppley-VGPM (Carr et al., 2006) and the CbPM (Westberry et al., 2008).

The global climatology of mixed layer depth (MLD) was taken from IFREMER/LOS (www.ifremer.fr/cerweb/deboyer/mld), which is computed at 2° spatial resolution. It is estimated (following De Boyer Montégut et al., 2004) from 5 million temperature profiles taken over the period 1990–2008.

In-situ dissolved inorganic nitrogen (DIN) concentrations were obtained from the World Ocean Database 2018 (Boyer et al., 2018) which is a product of NOAA's National Centre for Environmental Information (NCEI) and comprises a selection of quality-controlled oceanic profiles. Due to the spatially- and temporally-limited availability of observed DIN concentrations around the study area, all available observations were used from 1963 to 2019 instead of using a climatology.

3. Results

3.1. Model validation and Agulhas Bank characteristics

To assess the model's ability to simulate the circulation over the Agulhas Bank region, modelled surface currents were compared with those derived from satellite altimetry (absolute geostrophic velocities), shown as a decadal mean (Fig. 2). The mean speed and width of the AC are comparable with satellite observations along with weaker, but still visible, westward flow on the Agulhas Bank. Good qualitative agreement is also seen at monthly and annual timescales (Fig. S1). Key features of the Agulhas system, i.e., the position of the Agulhas Current (AC), its retroflection, and the level of mesoscale variability in the Agulhas Return Current (ARC), are known problems for global and regional models of varying resolution (e.g., Penven et al., 2010). In Fig. S1 these features are seen to be well represented with Fig. 2 also revealing similar values for EKE, which implies that a good agreement of the level of mesoscale variability exists between the model and AVISO. An important caveat is that while the model is run under reanalysis with forcing for each year, we do not expect the flow field to be directly comparable for specific

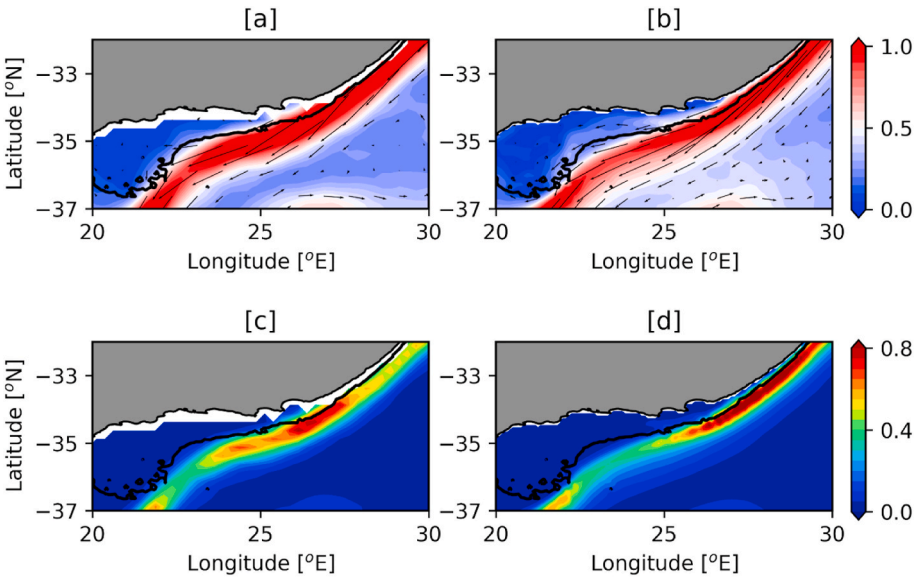

Fig. 2. Surface currents (m s^{-1}) and eddy kinetic energy (m s^{-1}) derived from altimetry [a, c] and the model [b, d] shown as a decadal mean from 2001 to 2010 over the Agulhas Bank. The black line represents the 200 m isobath.

months or years due to the chaotic nature of ocean flows. For example, although the model is clearly able to simulate meanders and eddies (as in January 2005), they do not necessarily occur in the same place as the observations (see Srokosz et al., 2015 and Jacobs et al., 2020 for similar challenges).

As shown in Fig. 3, for all seasons the model adequately simulates the overall spatial pattern and seasonal variability of SST in the selected domain, although generally runs slightly cooler than the observations, especially in the summer months (DJF and MAM). Year-round, a warm AC is evident along the edge of the shelf with cooler temperatures on the Agulhas Bank. The latter is particularly apparent further west, which is influenced by upwelling south of Cape Agulhas (Hutchings et al., 2009). On the CAB (Fig. 4), the model simulates the seasonal cycle well with the lowest SST (16°C) in August (attributed to winter mixing) and warmest in February (20.5°C; Fig. 4a). As seen in both the model and satellite observations, there is evidence of the CR from December to May, with cooler water protruding from the coast and orientated along the 100 m isobath (Fig. 3). On the EAB, temperatures are much cooler year-round, with evidence of upwelling along the coast which is more pronounced in the model, notably near Port Alfred and Port Elizabeth (now named Gqeberha). This could be due to the coarse resolution of the wind forcing which may affect the model's ability to adequately resolve smaller-scale coastal processes, or an overestimation of wind strength in the forcing dataset. The seasonal cycle here is similar to that observed on the CAB

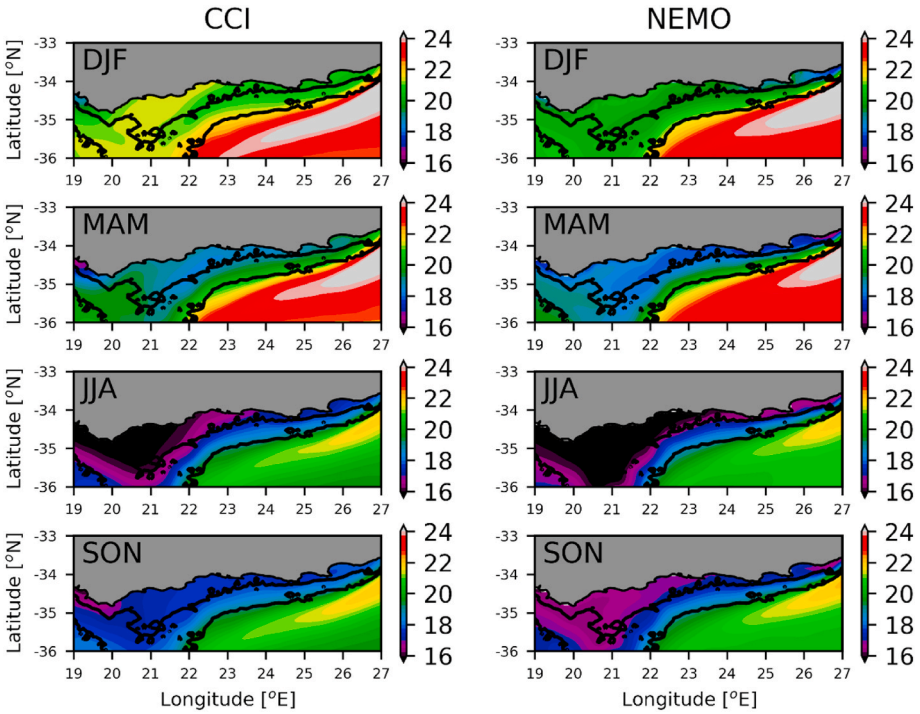

Fig. 3. Climatological SST (°C) in CCI (left) and the model (right) averaged over the period 1992–2010 for seasons defined as Dec–Feb (DJF), Mar–May (MAM), Jun–Aug (JJA) and Sep–Nov (SON). The black lines represent the 100 m and 200 m isobaths.

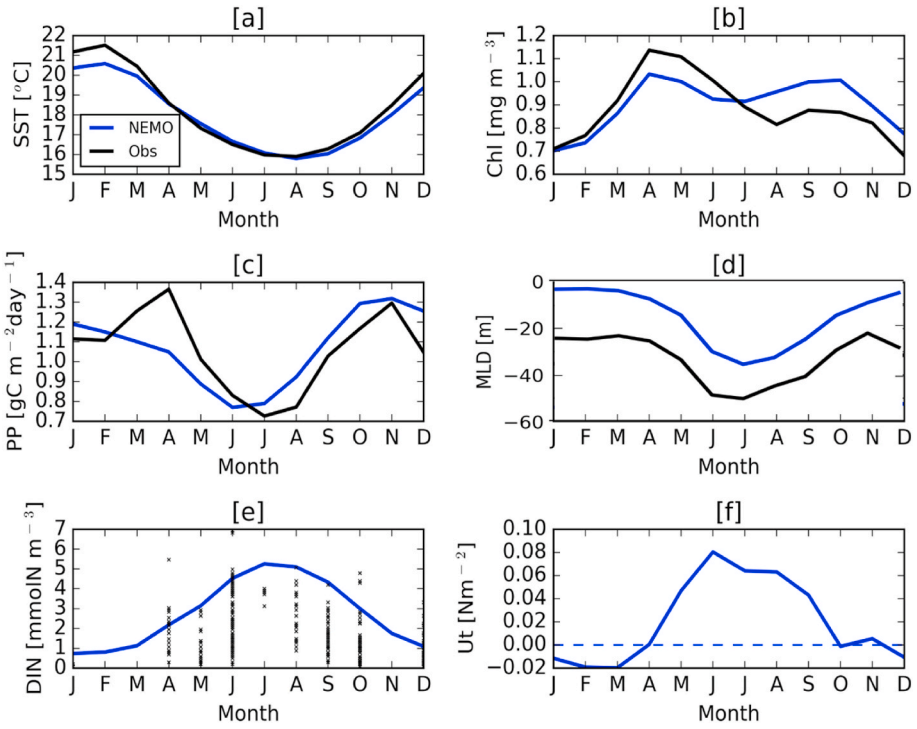

Fig. 4. Climatological seasonal cycle of SST [a; °C], Chl-*a* [b; mg m^{-3}], PP [c; gC m^{-2} day^{-1}], MLD [d; m], DIN [e; mmol m^{-3}] and zonal wind stress [f; Nm^{-2}] on the CAB, defined as the region from 21.25 to 24°E and from the coast to the 200 m isobaths (Fig.1). Blue lines indicate model. Black lines (markers in e) observations (see section 2.3 for details). Model fields are calculated from 1993 to 2015 (see section 2.3 for details on observational fields). Dashed line in f marks 0 Nm^{-2} to distinguish between westerly and easterly wind stress.

but, overall, the model tends to underestimate the temperature in summer and overestimate it in winter (Fig. S2a).

The seasonal variability of satellite and modelled chl-*a* for the Agulhas Bank is shown in Fig. 5. Overall, modelled chl-*a* concentrations are higher in the open ocean (i.e., off the shelf) by about 0.2 mg m^{-3} while underestimated along the coast, notably west of 25°E. Note the narrow coastal strip of elevated chl-*a* between 21 and 24°E which is driven by small cells of coastal upwelling (Walker, 1986). Despite the underestimation of chl-*a* on the shelf during summer and autumn (Fig. 4b; CAB and S2b; EAB), the model still simulates high concentrations on the EAB that extend westward along the path of the CR. In the long-term average, the modelled CR may extend slightly further south than seen from satellite observations but, overall, it is well represented in the climatology.

Overall, fairly good model performance is also seen for IntPP, MLD and surface DIN concentrations on the CAB with the magnitude and

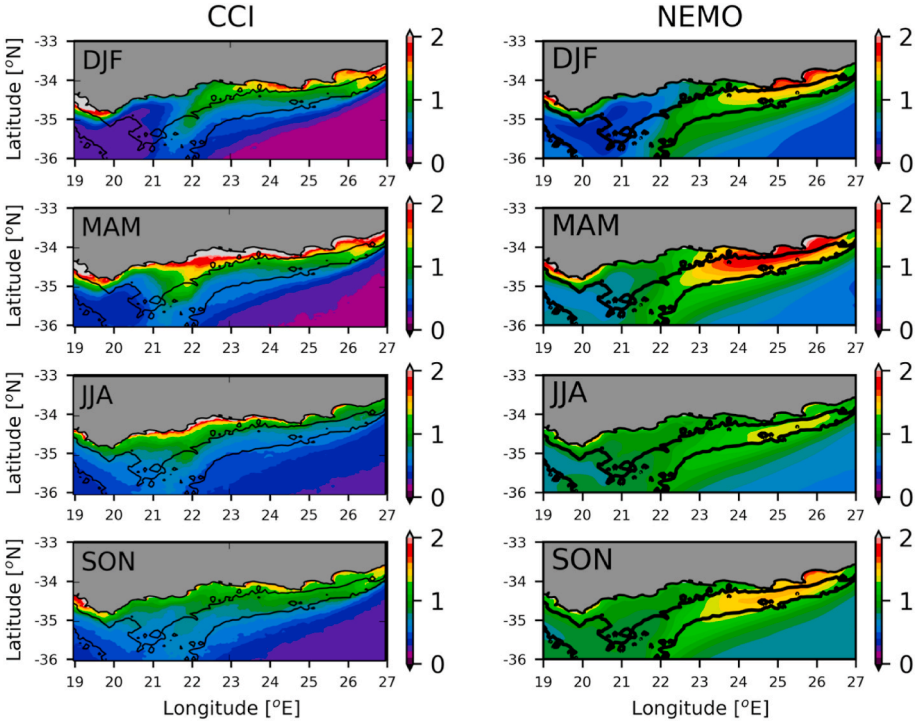

Fig. 5. Climatological *Chl-a* (mg m^{-3}) in CCI (left) and the model (right) averaged over the period 1998–2015 from Dec–Feb (DJF), Mar–May (MAM), Jun–Aug (JJA) and Sep–Nov (SON). The black lines represent the 100 m and 200 m isobaths.

seasonal range comparable to observations (Fig. 4). The modelled seasonal cycle of IntPP is similar to estimates based on remote sensing but the April peak, not found in the model, may be due to the subsurface maximum at this time of year. Modelled MLD is not as deep as that observed but the seasonal variability is captured. This difference in magnitudes may be due to the coarse resolution of the wind forcing (0.7°) in the model but it could also be due to the even coarser resolution of the observed climatology (2°) which may not be representative of the Agulhas Bank. The limited availability of DIN measurements in this region (see section 2.3) means that the climatology on the CAB is unable to be computed, hence all available observations are shown in Fig. 4e. The wide spread of data makes it difficult to interpret how well the model captures the seasonal variability but it is noteworthy that the magnitudes are in the same range. Similar comparisons are found on the EAB but with even fewer observed DIN measurements and a larger difference between the modelled and observed MLD (Fig. S2). This is most likely due to the low resolution of the observed MLD climatology which includes a considerable part of the ocean to the southeast of the EAB, making it difficult to make direct comparisons.

While the model may not be able to adequately resolve small-scale processes (i.e., at the coast on the EAB), the results above allow us to conclude that the model is able to adequately simulate the climatological spatial pattern, including the position and strength of the CR, and the seasonal variability of the key dynamic and biogeochemical properties.

3.2. Productivity on the Agulhas Bank and cold ridge

In addition to the model being able to represent the climatological spatial pattern and seasonal cycle of SST and chl-*a* on the Agulhas Bank, scrutiny of all years showed high variability at monthly timescales. Fig. 6 shows SST and surface chl-*a* for the most pronounced observed (April 2004; a,b) and modelled (April 1997; c,d) productive events in the time-series 1993–2015. We refer to these as 'strong' events as highly productive (chl-*a* concentrations >2.5 mg m^{-3}, compared with ~1.5 mg m^{-3} in the climatology – see Fig. 5) features are present on the Bank. In both events in Fig. 6, there is evidence of coastal upwelling with lower SSTs (<18°C, compared with >19°C in the climatology – see Fig. 3) and concomitant high chl-*a* concentrations (>3 mg m^{-3}) between Tsitsikamma and Port Alfred. The CR is also visible as a cool, highly productive filament extending south-westward from the coast, aligned with the 100 m isobath, and in agreement with other findings (e.g., Boyd and Shillington, 1994; Roberts and Van den Berg, 2002; Roberts 2005).

At the other end of the variability scale, Fig. S3 shows the most unproductive 'weak' events where SSTs on the shelf exceed 22°C and chl-*a* concentrations of 0–1 mg m^{-3} are found with a weak or non-existent CR. Both "strong" and "weak" events were chosen as the most pronounced productive or unproductive events as they are used to show that the model can represent both kinds of events adequately.

As discussed in section 3.1, when making comparisons between observational and model data, it is important to remember that although the model is externally forced under reanalysis datasets for the same period, model event timing does not necessarily correlate with the observed variability. Thus, when specific years or events are referred to in our results, they represent 'model' years. With this in mind, however, we note that the model is clearly able to simulate the main productive features on the Agulhas Bank, especially in terms of their strength, position and temporal variability (see Fig. S4 for monthly mean chl-*a* concentrations in April from 2001-10).

The surface upwelling seen on the EAB underpinning the strong April 1997 model event in Fig. 6 c,d is also viewed at the subsurface in Fig. 7. Near Port Elizabeth (Fig. 7a–c) isotherms slope upwards by > 150 m from 34.6 to 34°S with nutrient-rich water brought closer to the surface, culminating in surface chl-*a* concentrations of up to 2 mg m^{-2} near the coast. Further west in the vicinity of the CR, the doming of isotherms is viewed mid-shelf (Fig. 7d), which is consistent with previous findings (e.g., Swart and Largier, 1987; Boyd and Shillington, 1994), leading to SSTs of <17°C along the 100 m isobath (Fig. 6c). Surface DIN concentrations of >2 mmol m^{-3} are observed across the shelf with a chl-*a* maximum of >2.5 mg m^{-3} from 0 to 30 m – concurrent with the doming isotherms situated away from the coast. In the mean (Fig. S5), it is clear that upwelling mostly occurs on the EAB during summer, with similar chl-*a* concentrations found near the coast. Note in Fig. S5d that the mid-shelf doming due to the CR is not as pronounced, indicating the high variability of the CR feature.

In contrast, during a weak event (Fig. S3) there is evidence of reduced upwelling on the EAB with warm water (>18°C) at the surface and, as in the strong event, a subsurface chl-*a* maximum (Fig. S6b), though not as extensive as in the strong event (Fig. 7b). On the CAB, the CR signature is weak at the surface (Fig. S3), and while isothermal doming is visible at the subsurface, it is much weaker with a well-established upper mixed layer and a lower chl-*a* maximum, i.e., ~1.5 mg m^{-3} (Fig. S6).

From these results we conclude that upwelling on the EAB, certainly on monthly/climatological timescales, is a semi-permanent feature during summer but varies in strength, while the CR is not a stable feature and shows high interannual variability.

3.3. Dynamical links between the EAB and CAB

3.3.1. EAB wind stress and CAB productivity

We have shown that the EAB is dominated by coastal upwelling which transports cool, nutrient-rich water to the surface, while, in contrast, the CAB is dominated by the CR.

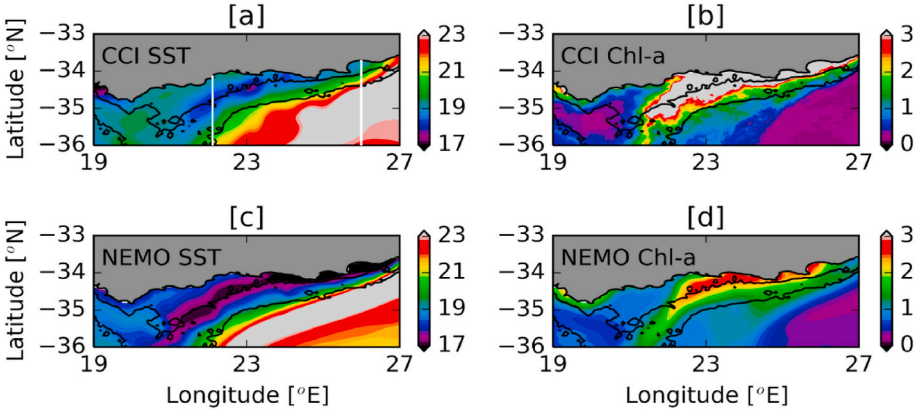

Fig. 6. SST [°C] and chl-*a* [mg m^{-3}] patterns in CCI (April 2004) [a, b] and the model (April 1997) [c, d] during strong productive events. The black lines represent the 100 m and 200 m isobaths. Vertical white lines denote the locations of the transects shown in Fig. 7.

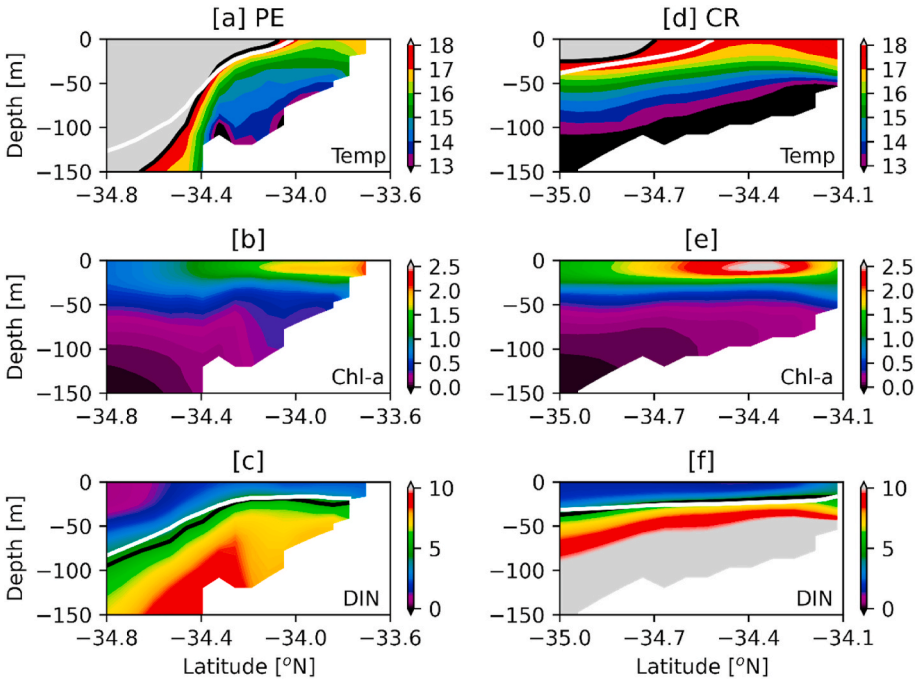

Fig. 7. Model vertical cross-sections of temperature [°C; a, d], chl-*a* [mg m^{-3}; b, e] and DIN [mmol m^{-3}; c; f] near Port Elizabeth (PE; at 26°E) and through the cold ridge (CR; at 22°E during the April 1997 high productivity event. Black and white lines [a,d] are the 18°C isotherm for April 1997 and the climatology (April 1993–2015) and the black and white lines on [c, f] are the 5 mmol m^{-3} contours for April 1997 and the climatology (April 1993–2015). See Fig. 6 for cross-section locations.

To investigate relationships between variables as well as the inter-annual variability and connectivity in both regions, we used the anomalous (monthly mean removed) modelled monthly mean zonal wind stress, SST, surface DIN, surface chl-*a*, IntPP and surface zonal currents, all shown in Fig. 8 (domains defined as in Fig. 1, i.e., the area <200 m and within 24-28°E (EAB) and 21.25–24°E (CAB) respectively) from November–April (summer) when the CR is usually observed. As was shown in Fig. 4f, this time of the year coincides with the dominant easterly winds in the region which induce wind-driven Ekman upwelling along the coast. Accordingly, Fig. 8a shows the anomalous zonal wind stress over the EAB which is seen to be positively correlated to SST (Fig. 8b) and negatively correlated to surface DIN concentrations on the EAB (Fig. 8c). Clear examples of this strong correlation occur during the summers of 1995-96 and 2010-11 with anomalous SSTs and DIN concentrations of −2.1°C and +2.4 mmol m^{-3} respectively, both exceeding the ±1 standard deviation (Fig. 8). While these events lead to peaks in chl-*a* and IntPP on the EAB (plots not shown), correlations with EAB zonal wind stress are greater for the CAB (Fig. 8d and e; Table 1). Importantly, the anomalous peaks in chl-*a* and IntPP during the summers of 1995-96 and 2010-11 of up to +1.1 mg m^{-3} and +0.35 gC m^{-2} d^{-1} respectively, are both associated with well-defined CRs such as shown in Fig. 6.

Quantitatively, the full analysis of correlation coefficients between these parameters is shown in Table 1 and corroborates the strongest relationships with zonal wind stress are SST and DIN on the EAB at a 0-month lag, and also a strong 1-month lag with chl-*a* and IntPP on the

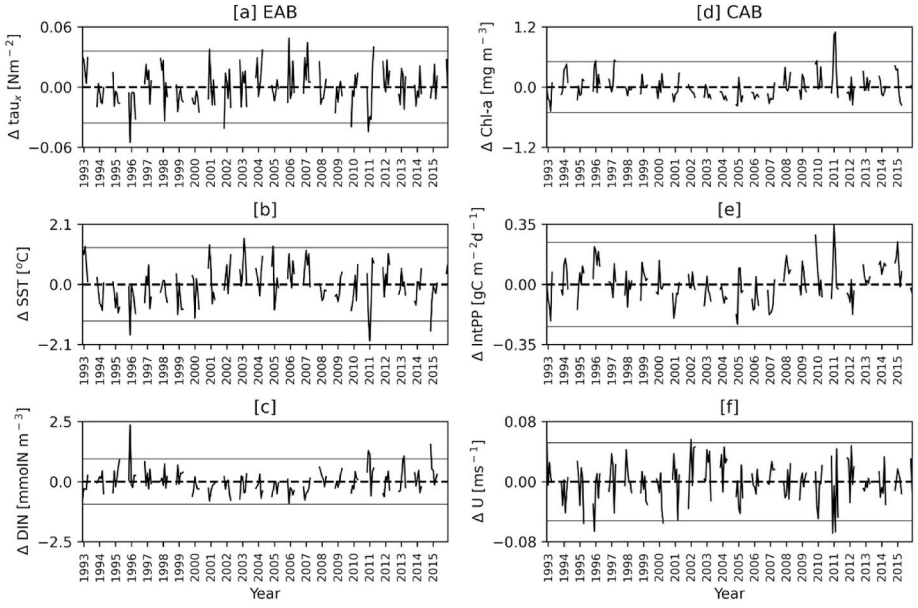

Fig. 8. Anomalous monthly summer (Nov–Apr) zonal wind stress [a; Nm^{-2}], SST [b; °C], DIN [c; mmol m^{-3}] on the EAB (23-28°E, <200 m) and mean chl-a [d; mg m^{-3}], Pr [e; gC m^{-2} d^{-1}] and zonal currents [f; ms^{-1}] on the CAB (21.25–23°E, <200 m) from 1993 to 2015 in NEMO. Horizontal lines indicate ± 1 standard deviation.

Table 1
Correlation coefficient (r) of the mean zonal wind (tau_x) from November to April (1993–2015) over the EAB (24-27°E, <200 m) with the mean SST and DIN over the EAB and mean chl-a and IntPP over the CAB (21.25–24°E, <200 m) at 0-month lag and +1-month lag (tau_x leads other variables). Values in bold are significant at the 95% level.

EAB tau_x	EAB SST		EAB DIN		CAB chl-a		CAB Pr	
	0 mon	+1 mon	0 mon	+1 mon	0 mon	+1 mon	0 mon	+1 mon
Nov	0.35	0.56	−0.25	−0.58	−0.36	−0.66	−0.43	−0.47
Dec	0.79	0.03	−0.75	0.1	−0.57	−0.09	−0.58	0
Jan	0.72	0.49	−0.47	−0.4	−0.51	−0.69	−0.27	−0.75
Feb	0.45	0.6	−0.48	−0.43	−0.48	−0.52	−0.38	−0.42
Mar	0.69	0.1	−0.72	0.1	−0.51	−0.44	−0.4	−0.29
Apr	0.55	0.5	−0.15	−0.37	−0.17	−0.57	−0.19	−0.39

CAB. However, in November the highest correlation is at a 1-month lag for all variables, most likely due to it being the beginning of the upwelling season. The opposite occurs in December, with the highest correlations occurring at 0-month lag across the shelf.

Of particular interest in this correlational analysis is the fact that the anomalous EAB easterly winds, apart from local impacts (i.e., the strong correlations with SST and DIN, indicating that they drive upwelling on the EAB), are also strongly correlated to positive chl-*a* and IntPP on the CAB with a 0-1-month lag.

3.3.2. *Is westward advection the connection?*

The 0-1-month lag between the zonal wind stress on the EAB and the chl-*a* and IntPP on the CAB could suggest mechanisms other than wind-driven upwelling are at play. Fig. 8f shows the anomalous zonal currents averaged over the CAB, and highlights anomalously strong westward (negative) flow on the shelf during highly productive events seen in Fig. 8e. This is supported by significant correlations during some months (Supp. Table 1). Specifically, strong negative correlations between zonal currents on the EAB and surface DIN (up to −0.56 in November, +1-month lag) and chl-*a* concentrations (up to −0.67 in April, +1-month lag) on the CAB. As noted earlier, the climatological flow on the Agulhas Bank is westward (which agrees with observations by Boyd et al., 1992; Hancke et al., this issue), so anomalies will indicate changes in flow strength rather than direction. This could suggest that strong flow events facilitate advection of near surface nutrients westward, enhancing phytoplankton blooms towards and on the CAB.

To explore this possibility further, we used a Lagrangian modelling approach where virtual (neutrally buoyant) particles were released during a strong and weak advection event. The events shown were selected as they represent clear examples of the influence of the currents on the Bank. Fig. 9a shows trajectories of particles released in the main upwelling region (yellow shade) on the EAB during a strong event in February 2011. This release area also corresponds to the chokka squid spawning grounds shown as red shade in Fig. 1. In this simulation, particles are seen to reach the CAB within six days before continuing either south-westward off the Bank (after ~18 days), or flowing westward along the coast to reach the Benguela upwelling system approximately one month later. Fig. 9b reveals the westward flow field on the Bank underpinning this advection with speeds of 0.5–0.75 m s^{-1}. These are in good agreement with ship ADCP measurements (Roberts, 2005; see his Fig. 9b). Filaments/patches of high DIN concentrations on the EAB show that the nutrient-rich water, upwelled mostly east of 25°E (Fig. 9c), must be advected in the westward flow, which results in higher concentrations than in surrounding waters further offshore between the 100–200 m isobaths. This advection appears to be an additional factor facilitating the large phytoplankton bloom (chl-a > 2.5 mg m^{-3}) in the

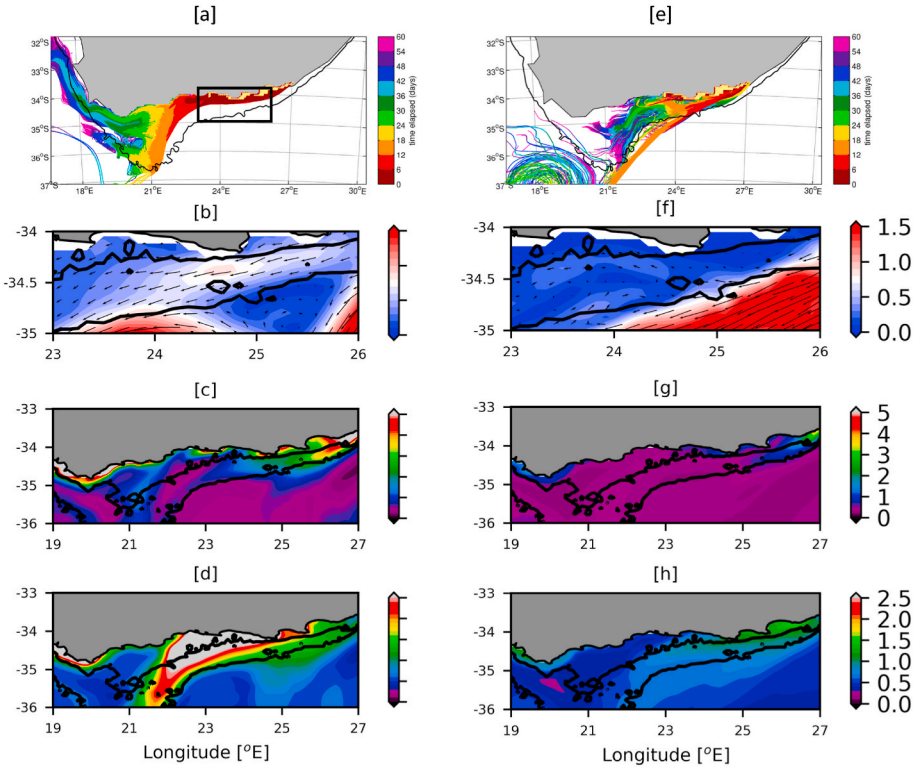

Fig. 9. Trajectories of 1470 particles released in the shaded yellow area on the EAB (a, e) during strong [b] and weak [f] shelf advection events in February 2011 and December 2000 respectively. Particles released at the beginning of February 2011 and December 2000 are advected in the model velocity field for 60 days (each colour in panel a and e represents the position of the particles every six days after deployment). Surface current speed in b and f is m s^{-1}. Corresponding surface DIN concentrations (mmol m^{-3}) are shown as five-day means in c and g with surface chlorophyll-*a* concentrations (mg m^{-3}) in d and h, both at the beginning of February 2011 and December 2000. Black lines indicate the 100 m and 200 m isobaths.

vicinity of the CR on the CAB (Fig. 9d). It is also worth noting that a Natal Pulse is present during this event, which may lead to enhanced upwelling on the Bank (Goschen et al., 2015), and is also observed by Krug et al. (2014). The changes in flow on the Bank caused by the passage of a Natal Pulse (addressed in Jacobs et al. *this issue*) may also promote the advection of nutrients towards the CAB.

In contrast to the strong event of February 2011, the flow pattern of the trajectories during the weak event in December 2000 indicates two main pathways (Fig. 9e). Some particles flow westward across the Bank, taking at least 18 days to reach the CAB, which is three times slower than in February 2011. For the other pathway, a considerable proportion of particles (nearly 40%) are advected in a south-westward direction off the shelf with the AC, crossing the shelf edge after one to two weeks. Fig. 9f shows the underlying weak circulation with currents of <0.5 m s^{-1}. The corresponding surface spatial pattern of DIN (Fig. 9g) indicates little upwelling and oligotrophy on the EAB, and very low levels of chl-*a* over the entire shelf (Fig. 9h).

While this analysis, and that in Section 3.3.1, are snap-shots, they do point to a role, and possible consequence, of the dominantly westward shelf circulation over the EAB. Namely, during strong current events, the advection of upwelled nutrient-rich water on the EAB (i.e. Fig. 7 a,b,c) can further enhance productivity on the CAB, already driven by the CR.

4. Discussion

This study employs a high-resolution biogeochemical model (NEMO-MEDUSA at 1/12°) to investigate the mechanisms driving productivity on the Agulhas Bank. Prior studies have been unable to provide the spatial and temporal resolution to investigate interannual variability of IntPP on the Agulhas Bank and fail to segregate between the Eastern Agulhas Bank (EAB) and Central Agulhas Bank (CAB; e.g., Probyn et al., 1994). Additionally, it is known that the Cold Ridge (CR) is a central feature on the CAB (e.g., Boyd and Shillington 1994; Roberts and Van den Berg, 2002; Roberts, 2005) but these studies are also strongly constrained by limited spatial and temporal data coverage. Here, the analysis is based on monthly mean climatologies from 1993 to 2015 (23 years), distinguishes between the EAB and CAB, and pays special attention to the CR feature.

In the long-term (>20 years) mean, peak productivity occurs in April (Fig. 4), with elevated chl-a concentrations found on the EAB and CAB in spring and summer (Figs. 3 and 5). During this period, there is evidence of the CR in the remotely sensed SST and chl-a climatology along the 100 m isobath. Thus far, previous modelling studies have found some evidence for the CR with a slight doming of climatological isotherms on the CAB (Chang, 2008). This signal is also apparent in NEMO-MEDUSA but with additional evidence of elevated chl-a concentrations, indicative of the CR.

In addition to being able to represent the overall climatological spatial pattern of SST and chl-a, the model is also able to simulate CR events on monthly timescales with its position, extent and strength comparable to that observed in satellite remote sensing. This is the first time such events have been explored over a long time period (>20 years) in terms of the physical and biogeochemical aspects of the CR, with the model enabling subsurface analysis. The slight doming seen in the climatology (Fig. S5) is much more pronounced at the event-scale and resembles observed temperature sections (e.g., Boyd and Shillington, 1994). This doming is also associated with high chl-a concentrations in the upper ~30 m. However, there are some differences between the spatial pattern of SST and chl-*a*, and the wind-driven upwelling is more pronounced in the model which may overestimate the correlations. Thus, it may require the use of a higher resolution model than used in this study to understand the mesoscale dynamics which may modulate the degree of upwelling on the Bank.

Occurrences of the CR were visible during the period November to April, with considerable interannual variability in its strength, i.e., its productivity. A number of "strong events" occurred with chl-a concentrations exceeding 2.5 mg m^{-3} while there were some months where the CR was weak or even absent. Variability is also found in the shape and position of the CR, with the traditional extension along the 100 m isobath not always apparent. Nevertheless, the highest productivity events on the CAB are associated with the existence of a prominent CR.

Prior studies have focussed on what mechanisms are responsible for the cold bottom water on the shelf, namely shelf-edge upwelling in the bottom layer along the edge of the Agulhas Bank (Chang, 2008; Jackson et al., 2012), making the AC the primary mechanism for CR formation. Here, we find that interannual variability in other mechanisms, namely wind stress and advection, are also important drivers of interannual variability in the strength of the CR, which, in addition to be defined by temperature, can also be defined by primary production (Fig. 8). Anomalous easterly wind stress initiates intense upwelling at the coast on the EAB leading to cool, nutrient-rich waters being brought to the surface. Currents on the Bank then transport this water westwards, leading to large phytoplankton blooms on the CAB (0–1 month later), with the highest productivity in the vicinity of the CR. Lagrangian analysis showed the westward advection of nutrients to the CAB in under six days during a strong event, with the highest chl-a concentrations found in the path of the currents on the Bank. Conversely, during a weak event, the combination of low nutrient concentrations at the coast (from weak winds) and reduced connectivity to the CAB resulted in low chl-*a* concentrations on the CAB. The main mechanisms leading to enhanced productivity are summarized in Fig. 10.

These findings build on the work of Roberts (2005) who first proposed the westward transport hypothesis where chokka squid larvae utilise the westward currents to transport them from their optimal spawning grounds on the EAB to the feeding grounds on the CAB. Using remotely sensed SST, his analysis also indicated that currents may be vital for CR formation with wind-driven coastal upwelling alone not enough to initiate CR formation (Roberts, 2005). While the Lagrangian analysis provides more evidence for this hypothesis in terms of CR formation, the fact that productivity is not limited to the CR region may suggest that it is not as important as once believed for chokka squid paralarvae survival.

Productivity across the Bank remains vital for chokka survival and recruitment, and low productivity may have caused the low catches recorded in 2013. While we cannot directly assess individual years, the wind forcing is from a reanalysis dataset (includes interannual variability as opposed to a climatology forcing dataset) and represents the true synoptic scenario at the time. The year 2013 appears fairly normal with mixed winds and slightly anomalous primary production (Fig. 8). However, while 2012 doesn't stand out in terms of peak anomalies, it underwent persistent weak wind stress from November to April that resulted in anomalously negative chl-*a* concentrations and IntPP on the CAB for the entire period. This may have led to increased starvation of squid larvae, reducing recruitment for 2013 (see Bruggeman et al. (this issue) for details on the chokka squid life cycle).

5. Conclusions

Using a high-resolution biogeochemical ocean model, this study aimed to improve understanding of spatial and temporal variability of primary productivity on the Agulhas Bank, in particular the role of the CR, on seasonal and interannual timescales. The most productive events were found to be associated with a strong CR on the CAB. These events occurred alongside periods of intense easterly winds, with upwelling leading to strong cooling and high DIN concentrations on the EAB, with fast westward currents advecting these nutrients to the CAB within a few days, initiating large phytoplankton blooms. This is the first time physical and biogeochemical aspects of the CR have been simulated on monthly timescales, and this study builds on previous work by conducting a longer-term analysis than has been done before. It also provides further evidence that the CR is a feature tied to wind-driven

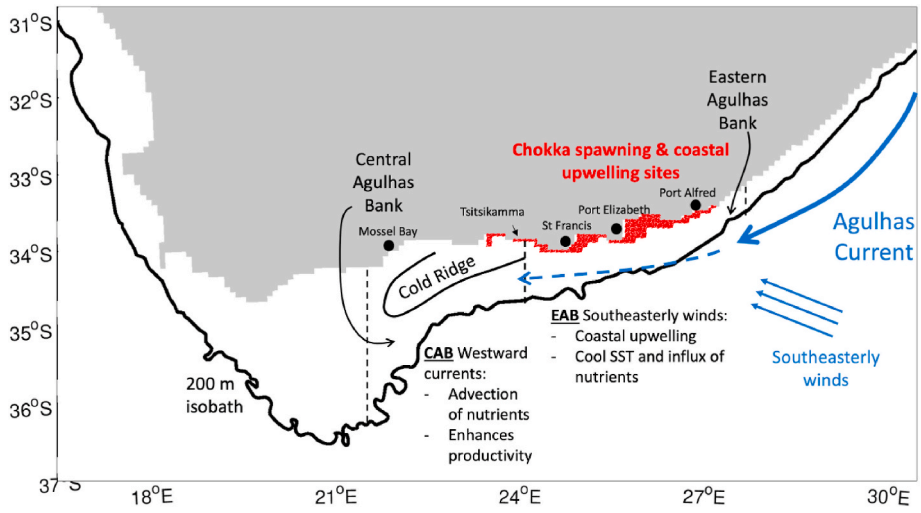

Fig. 10. Map of the Agulhas Bank, delineated by the 200 m isobath, summarizing the main driving mechanisms (in blue) resulting in high productivity events. Red shaded area demarcates the main chokka squid spawning grounds and upwelling sites.

upwelling and for the westward transport hypothesis (Roberts, 2005) with westward advection of nutrients important for CR formation and variability. There is some indication that a change in the physical regime occurred over the summers of 2010–11, leading to 2012 being an unusually weak year for primary production on the Bank. This may have affected chokka squid recruitment and catch in 2013. Additionally, if the prevailing currents lead to offshore losses, i.e., preventing the paralarvae from reaching the CR, this would also reduce recruitment and is explored in Jacobs et al. (this issue). Further work needs to be done to investigate the links between the local productivity and the chokka squid catch (see Jebri et al., 2022), which, if demonstrated, could lead to improved predictive capacity of variability in the catches.

Author contribution statement

Z.J. developed the original idea, produced description of the results and most of the key figures. E.P. contributed to the design of the Lagrangian particle tracking experiments, which were conducted by S.K. who also produced the trajectory figures. E.P., F.J., M.S., M.R., W.S. and J.B. contributed to the interpretation and discussion of the results. E.P. and M.R. contributed to the development of the idea. All authors contributed to the improvement of the paper, made edits and reviewed the final manuscript. E.P. coordinated the study.

Declaration of competing interest

The authors declare that they have no known competing financial interests or personal relationships that could have appeared to influence the work reported in this paper.

Acknowledgements

This publication was produced with the financial support of the Global Challenges Research Fund (GCRF) in the framework of the SOLSTICE-WIO project, NE/P021050/1. This work is also part of the UK-SA Bilateral Chair in Ocean Science and Marine Food Security funded by the British Council Newton Fund grant SARCI 1503261 16102/NRF98399. The altimeter products were produced by AVISO (http://www.aviso.altimetry.fr/en/data/products/sea-surface-height-products/gloabal/) as part of the SSALTO ground-processing segment. The authors wish to thank the Copernicus Marine Environment Monitoring Service (marine. copernicus.eu) for providing the absolute geostrophic currents. We acknowledge the NEMO consortium for the modelling framework used in this study. The model run was performed using the ARCHER UK National Supercomputing with outputs stored at the Centre for Environmental Data Analysis JASMIN servers and can be provided upon request. The Ariane software was developed by B. Blanke and N. Grima.

Appendix A. Supplementary data

Supplementary data to this article can be found online at https://doi.org/10.1016/j.dsr2.2022.105080.

References

Antonov, J., Locarnini, R., Boyer, T., Mishonov, A., Garcia, H., Levitus, S., 2006. World Ocean Atlas 2005 Volume 2: Salinity, 2. Noaa atlas nesdis.
Augustyn, C., Lipinski, M., Roberts, M., Mitchell-Innes, B., Sauer, W., 1994. Chokka squid on the Agulhas Bank: life history and ecology. South Afr. J. Sci. 90 (3).
Barlow, R., Lamont, T., Kyewalyanga, M., Sessions, H., Morris, T., 2010. Phytoplankton production and physiological adaptation on the southeastern shelf of the Agulhas ecosystem. Continent. Shelf Res. 30 (13), 1472–1486. https://doi.org/10.1016/j.csr.2010.05.007.
Beckley, L.E., 1983. Sea-surface temperature variability around Cape Recife, South Africa. South Afr. J. Sci. 79 (11), 436–438.
Behrenfeld, M.J., Falkowski, P.G., 1997. Photosynthetic rates derived from satellite-based chlorophyll concentration. Limnol. Oceanogr. 42 (1), 1–20.
Blanke, B., Raynaud, S., 1997. Kinematics of the Pacific equatorial undercurrent: an Eulerian and Lagrangian approach from GCM results. J. Phys. Oceanogr. 27 (6), 1038–1053. https://doi.org/10.1175/1520-0485(1997)027%3C1038:KOTPEU%3E2.0.CO;2.
Boyd, A.J., Trump, B.B.S., Horstmann, D.A., 1985. The hydrology off the South African south-western coast between Cape point and danger point in 1975. S. Afr. J. Mar. Sci. 3 (1), 145–168.
Boyd, A.J., Taunton-Clark, J., Oberholster, G.P.J., 1992. Spatial features of the near-surface and midwater circulation patterns off western and southern South Africa and their role in the life histories of various commercially fished species. S. Afr. J. Mar. Sci. 12 (1), 189–206. https://doi.org/10.2989/02577619209504702.
Boyd, A.J., Shillington, F.A., 1994. Physical forcing and circulation patterns on the Agulhas Bank. South Afr. J. Sci. 90 (3), 143–154. https://hdl.handle.net/10520/AJA00382353_4624.
Boyer, T.P., Baranova, O.K., Coleman, C., Garcia, H.E., Grodsky, A., Locarnini, R.A., et al., 2018. NOAA Atlas NESDIS 87. World Ocean Database.
Brodeau, L., Barnier, B., Treguier, A.M., Penduff, T., Gulev, S., 2010. An ERA40-based atmospheric forcing for global ocean circulation models. Ocean Model. 31 (3–4), 88–104.
Bryden, H.L., Beal, L.M., Duncan, L.M., 2005. Structure and transport of the Agulhas Current and its temporal variability. J. Oceanogr. 61 (3), 479–492.
Carr, M.E., Friedrichs, M.A., Schmeltz, M., Aita, M.N., Antoine, D., Arrigo, K.R., et al., 2006. A comparison of global estimates of marine primary production from ocean color. Deep Sea Res. Part II Top. Stud. Oceanogr. 53 (5–7), 741–770.
Chang, N., 2008. Numerical Ocean Model Study of the Agulhas Bank and the Cool Ridge.
Chapman, P., Largier, J.L., 1989. On the origin of Agulhas Bank bottom water. South Afr. J. Sci. 85 (8), 515–519.
DAFF, 2009. 2009/10 DAFF Strategic Plan. Department of Agriculture Forestry and Fisheries, Pretoria.

De Boyer Montégut, C., Madec, G., Fischer, A.S., Lazar, A., Iudicone, D., 2004. Mixed layer depth over the global ocean: an examination of profile data and a profile-based climatology. J. Geophys. Res.: Oceans 109 (C12). https://doi.org/10.1029/2004JC002378.

De Ruijter, W.P., Van Leeuwen, P.J., Lutjeharms, J.R., 1999. Generation and evolution of natal Pulses: solitary meanders in the Agulhas current. J. Phys. Oceanogr. 29 (12), 3043–3055.

Dussin, R., Barnier, B., Brodeau, L., Molines, J.M., 2016. Drakkar Forcing Set Dfs5. MyOcean Report.

Gill, A.E., Schumann, E.H., 1979. Topographically induced changes in the structure of an inertial coastal jet: application to the Agulhas Current. J. Phys. Oceanogr. 9 (5), 975–991.

Goschen, W.S., Schumann, E.H., Bernard, K.S., Bailey, S.E., Deyzel, S.H.P., 2012. Upwelling and ocean structures off Algoa Bay and the south-east coast of South Africa. Afr. J. Mar. Sci. 34 (4), 525–536. https://doi.org/10.2989/1814232X.2012.749810.

Goschen, W.S., Bornman, T.G., Deyzel, S.H.P., Schumann, E.H., 2015. Coastal upwelling on the far eastern Agulhas Bank associated with large meanders in the Agulhas Current. Continent. Shelf Res. 101, 34–46. https://doi.org/10.1016/j.csr.2015.04.004.

Hancke, L., Smeed, D., Roberts, M., Rayner, D., Jebri, F. and Russo, C. (under review). The structure and dynamics of the cold ridge on the central Agulhas Bank, South Africa. Deep Sea Res. Part II Top. Stud. Oceanogr..

Hsuesh, Y., O'Brien, J.J., 1971. Steady coastal upwelling induced by an along-shore current. J. Phys. Oceanogr. 1 (3), 180–186.

Huggett, J.A., Richardson, A.J., 2000. A review of the biology and ecology of Calanus agulhensis off South Africa. ICES (Int. Counc. Explor. Sea) J. Mar. Sci. 57 (6), 1834–1849. https://doi.org/10.1006/jmsc.2000.0977.

Hutchings, L., Barange, M., Bloomer, S.F., Boyd, A.J., Crawford, R.J.M., Huggett, J.A., et al., 1998. Multiple factors affecting South African anchovy recruitment in the spawning, transport and nursery areas. S. Afr. J. Mar. Sci. 19 (1), 211–225. https://doi.org/10.2989/025776198784126908.

Hutchings, L., 1992. Fish harvesting in a variable, productive environment—searching for rules or searching for exceptions? S. Afr. J. Mar. Sci. 12 (1), 297–318. https://doi.org/10.2989/02577619209504708.

Hutchings, L., Van der Lingen, C.D., Shannon, L.J., Crawford, R.J.M., Verheye, H.M.S., Bartholomae, C.H., et al., 2009. The Benguela Current: an ecosystem of four components. Prog. Oceanogr. 83 (1–4), 15–32.

IOCCG, 2000. IOCCG. In: Sathyendrannath, S. (Ed.), Remote Sensing of Ocean Colour in Coastal and Other Optically Complex Waters, 3. Reports of the International Ocean Colour Coordinating Group, Dartmouth, Canada, pp. 23–46. Chap. 2.

Jackson, J.M., Rainville, L., Roberts, M.J., McQuaid, C.D., Lutjeharms, J.R., 2012. Mesoscale bio-physical interactions between the Agulhas current and the Agulhas Bank, South Africa. Continent. Shelf Res. 49, 10–24.

Jackson, T., Sathyendranath, S., Mélin, F., 2017. An improved optical classification scheme for the Ocean Colour Essential Climate Variable and its applications. Remote Sens. Environ. 152–161. https://doi.org/10.1016/j.rse.2017.03.036, 203.

Jacobs, Z.L., Jebri, F., Raitsos, D.E., Popova, E., Srokosz, M., Painter, S.C., et al., 2020. Shelf-break upwelling and productivity over the North Kenya Banks: the importance of large-scale ocean dynamics. J. Geophys. Res.: Oceans 125 (1), e2019JC015519.

Jacobs, Z., Kelly, S., Jebri, F., Roberts, M., Srokosz, M., Sauer, W., Hancke, L. & Popova, E. (under review) Retention properties of the Agulhas Bank and their relevance to the chokka squid life cycle. Deep Sea Res. Part II Top. Stud. Oceanogr..

Jebri, F., Raitsos, D.E., Gittings, J.A., Jacobs, Z.L., Srokosz, M., Gornall, J., Sauer, W.H., Roberts, M.J., Popova, E., 2022. Unravelling links between squid catch variations and biophysical mechanisms in South African waters. Deep Sea Res. Part II Top. Stud. Oceanogr., 105028 https://doi.org/10.1016/j.dsr2.2022.105028.

Joyner, J.M., 2015. The Influence of Environmental Variability on the Catch of Chokka, loligo Reynaudii, off the Coast of South Africa. Rhodes University, South Africa, p. 108. Master's Thesis. http://vital.seals.ac.za:8080/vital/access/manager/PdfViewer/vital:24013/SOURCE1?viewPdfInternal=1.

Krug, M., Tournadre, J., Dufois, F., 2014. Interactions between the Agulhas Current and the eastern margin of the Agulhas Bank. Continent. Shelf Res. 81, 67–79. https://doi.org/10.1016/j.csr.2014.02.020.

Largier, J.L., Swart, V.P., 1987. East-west variation in thermocline breakdown on the Agulhas Bank. S. Afr. J. Mar. Sci. 5 (1), 263–272. https://doi.org/10.2989/025776187784522252.

Leber, G.M., Beal, L.M., Elipot, S., 2017. Wind and current forcing combine to drive strong upwelling in the Agulhas Current. J. Phys. Oceanogr. 47 (1), 123–134. https://doi.org/10.1175/JPO-D-16-0079.1.

Levitus, S., Conkright, M., Boyer, T.P., O'Brian, T., Antonov, J., Stephens, C., et al., 1998. World Ocean Database 1998. NOAA Atlas. Technical report NESDIS 18.

Lipinski, M.R., Van der Vyver, J.S.F., Shaw, P., Sauer, W.H.H., 2016. Life cycle of chokka squid, Loligo reynaudii, in South African waters. Afr. J. Mar. Sci. https://doi.org/10.2989/1814232X.2016.1230074.

Lutjeharms, J.R.E., Catzel, R., Valentine, H.R., 1989. Eddies and other boundary phenomena of the Agulhas Current. Continent. Shelf Res. 9 (7), 597–616.

Lutjeharms, J.R.E., Meyer, A.A., Ansorge, I.J., Eagle, G.A., Orren, M.J., 1996. The nutrient characteristics of the Agulhas Bank. S. Afr. J. Mar. Sci. 17 (1), 253–274. https://doi.org/10.2989/025776196784158464.

Lutjeharms, J.R.E., Cooper, J., Roberts, M., 2000. Upwelling at the inshore edge of the Agulhas current. Continent. Shelf Res. 20 (7), 737–761. https://doi.org/10.1016/S0278-4343(99)00092-8.

Lutjeharms, J.R., 2006. The Agulhas Current, 329. Springer, Berlin.

Madec, G., 2015. NEMO Ocean Engine.

Malan, N., Durgadoo, J.V., Biastoch, A., Reason, C., Hermes, J., 2019. Multidecadal wind variability drives temperature shifts on the Agulhas Bank. J. Geophys. Res.: Oceans 124 (5), 3021–3035. https://doi.org/10.1029/2018JC014614.

Marzocchi, A., Hirschi, J.J.M., Holliday, N.P., Cunningham, S.A., Blaker, A.T., Coward, A.C., 2015. The North Atlantic subpolar circulation in an eddy-resolving global ocean model. J. Mar. Syst. 142, 126–143. https://doi.org/10.1016/j.jmarsys.2014.10.007.

Mthembu, S.P., 2019. The Socio-Economic Impact of the Squid Stock Volatility in the Eastern Cape Province of South Africa. University of Cape Town, School of Economics, South Africa, p. 52. Master's Thesis. https://open.uct.ac.za/bitstream/handle/11427/31078/thesis_com_2019_mthembu_senzo_peter.pdf?isAllowed=y&sequence=1.

Miller, D.C., Moloney, C.L., van der Lingen, C.D., Lett, C., Mullon, C., Field, J.G., 2006. Modelling the effects of physical–biological interactions and spatial variability in spawning and nursery areas on transport and retention of sardine Sardinops sagax eggs and larvae in the southern Benguela ecosystem. J. Mar. Syst. 61 (3–4), 212–229.

Moat, B.I., Josey, S.A., Sinha, B., Blaker, A.T., Smeed, D.A., McCarthy, G., et al., 2016. Major variations in subtropical North Atlantic heat transport at short (5 day) timescales and their causes. J. Geophys. Res.: Oceans 121, 3237–3249. https://doi.org/10.1002/2016JC011660.

Parada, C., Van Der Lingen, C.D., Mullon, C., Penven, P., 2003. Modelling the effect of buoyancy on the transport of anchovy (Engraulis capensis) eggs from spawning to nursery grounds in the southern Benguela: an IBM approach. Fish. Oceanogr. 12 (3), 170–184. https://doi.org/10.1046/j.1365-2419.2003.00235.x.

Penven, P., Cambon, G., Tan, T.A., Marchesiello, P., Debreu, L., 2010. ROMS AGRIF/ROMSTOOLS.

Peterson, W.T., Hutchings, L., Huggett, J.A., Largier, J.L., 1992. Anchovy spawning in relation to the biomass and the replenishment rate of their copepod prey on the western Agulhas Bank. S. Afr. J. Mar. Sci. 12 (1), 487–500. https://doi.org/10.2989/02577619209504720.

Popova, E., Yool, A., Byfield, V., Cochrane, K., Coward, A.C., Salim, S.S., et al., 2016. From global to regional and back again: common climate stressors of marine ecosystems relevant for adaptation across five ocean warming hotspots. Global Change Biol. 22 (6), 2038–2053. https://doi.org/10.1111/gcb.13247.

Probyn, T.A., Mitchellinnes, B.A., Brown, P.C., Hutchings, L., Carter, R.A., 1994. Review of Primary Production and Related Processes on the Agulhas-Bank.

Racault, M.F., Sathyendranath, S., Brewin, R.J., Raitsos, D.E., Jackson, T., Platt, T., 2017. Impact of El Niño variability on oceanic phytoplankton. Front. Mar. Sci. 4, 133. https://doi.org/10.3389/fmars.2017.00133.

Roberts, M.J., Van den Berg, M., 2002. Recruitment variability of chokka squid (Loligo vulgaris reynaudii)—role of currents on the Agulhas Bank (South Africa) in paralarvae distribution and food abundance. Bull. Mar. Sci. 71 (2), 691–710.

Roberts, M.J., 2005. Chokka squid (Loligo vulgaris reynaudii) abundance linked to changes in South Africa's Agulhas Bank ecosystem during spawning and the early life cycle. ICES (Int. Counc. Explor. Sea) J. Mar. Sci. 62 (1), 33–55.

Roberts, M.J., Van den Berg, M., 2005. Currents along the Tsitsikamma coast, South Africa, and potential transport of squid paralarvae and ichthyoplankton. Afr. J. Mar. Sci. 27 (2), 375–388. https://doi.org/10.2989/18142320509504096.

Rouault, M.J., Penven, P., 2011. New perspectives on Natal Pulses from satellite observations. J. Geophys. Res.: Oceans 116 (C7). https://doi.org/10.1029/2010JC006866.

Roughan, M., Middleton, J.H., 2002. A comparison of observed upwelling mechanisms off the east coast of Australia. Continent. Shelf Res. 22 (17), 2551–2572. https://doi.org/10.1016/S0278-4343(02)00101-2.

Roy, C., Van der Lingen, C.D., Coetzee, J.C., Lutjeharms, J.R.E., 2007. Abrupt environmental shift associated with changes in the distribution of Cape anchovy Engraulis encrasicolus spawners in the southern Benguela. Afr. J. Mar. Sci. 29 (3), 309–319. https://doi.org/10.2989/AJMS.2007.29.3.1.331.

Russo, C.S., Lamont, T., Tutt, G.C.O., van den Berg, M.A., Barlow, R.G., 2019. Hydrography of a shelf ecosystem inshore of a major Western Boundary Current. Estuar. Coast Shelf Sci. 228, 106363 https://doi.org/10.1016/j.ecss.2019.106363.

Schumann, E.H., 1986. The bottom boundary layer inshore of the Agulhas Current off Natal in August 1975. S. Afr. J. Mar. Sci. 4 (1), 93–102.

Schumann, E.H., Perrins, L.A., Hunter, I.T., 1982. Upwelling along the south coast of the Cape Province, South Africa. South Afr. J. Sci. 78, 238–242.

Schumann, E.H., Ross, G.J.B., Goschen, W.S., 1988. Cold water events in Algoa Bay and along the Cape south coast, South Africa, in March/April 1987. South Afr. J. Sci. 84, 579–584.

Schumann, E.H., 1992. Interannual wind variability on the South and East Coasts of South Africa. J. Geophys. Res. 97 (D18), 20,397–30, 403.

Schumann, E.H., Cohen, A.L., Jury, M.R., 1995. Coastal sea surface temperature variability along the south coast of South Africa and the relationship to regional and global climate. J. Mar. Res. 53 (2), 231–248. https://doi.org/10.1357/0022240953213205.

Shannon, L.V., Hutchings, L., Bailey, G.W., Shelton, P.A., 1984. Spatial and temporal distribution of chlorophyll in southern African waters as deduced from ship and satellite measurements and their implications for pelagic fisheries. S. Afr. J. Mar. Sci. 2 (1), 109–130. https://doi.org/10.2989/02577618409504363.

Srokosz, M.A., Robinson, J., McGrain, H., Popova, E.E., Yool, A., 2015. Could the Madagascar bloom be fertilized by Madagascan iron? J. Geophys. Res.: Oceans 120, 5790–5803. https://doi.org/10.1002/2015JC011075.

Swart, V.P., Largier, J.L., 1987. Thermal structure of Agulhas Bank water. S. Afr. J. Mar. Sci. 5 (1), 243–252.

US Department of Commerce, 2006. National Oceanic and Atmospheric Administration. In: 2-minute gridded global relief data (ETOPO2v2). National Geophysical Data Center.

Walker, N.D., 1986. Satellite observations of the Agulhas Current and episodic upwelling south of Africa. Deep Sea Res. Part A. Oceanographic Research Papers 33 (8), 1083–1106. https://doi.org/10.1016/0198-0149%2886%2990032-4.

Westberry, T., Behrenfeld, M.J., Siegel, D.A., Boss, E., 2008. Carbon-based primary productivity modeling with vertically resolved photoacclimation. Global Biogeochem. Cycles 22 (2). https://doi.org/10.1029/2007gb003078.

Yamagami, Y., Tozuka, T., Qiu, B., 2019. Interannual variability of the natal Pulse. J. Geophys. Res.: Oceans 124 (12), 9258–9276. https://doi.org/10.1029/2019JC015525.

Yool, A., Popova, E.E., Anderson, T.R., 2013. MEDUSA-2.0: an intermediate complexity biogeochemical model of the marine carbon cycle for climate change and ocean acidification studies. Geosci. Model Dev. (GMD) 6 (5), 1767–1811. https://doi.org/10.5194/gmd-6-1767-2013.

Yool, A., Popova, E.E., Coward, A.C., 2015. Future change in ocean productivity: is the Arctic the new Atlantic? J. Geophys. Res.: Oceans 120 (12), 7771–7790. https://doi.org/10.1002/2015JC011167.